Localized density enhancements in the magnetosheath: Three-dimensional morphology and possible importance for impulsive penetration

T Karlsson, N Brenning, H Nilsson, Jean-Gabriel Trotignon, Xavier Vallières, G Facsko

Localized density enhancements in the magnetosheath: Three-dimensional morphology and possible importance for impulsive penetration

T. Karlsson,[1] N. Brenning,[1] H. Nilsson,[2] J.-G. Trotignon,[3] X. Vallières,[3] and G. Facsko[4,5]

Received 14 August 2011; revised 6 February 2012; accepted 12 February 2012; published 31 March 2012.

[1] We use Cluster multipoint density measurements, using the spacecraft potential, to identify localized density enhancements (>50%) in the magnetosheath, and estimate their three-dimensional morphology and orientation. Typically one dimension of the density enhancements is shorter than others, is directed perpendicular to the background magnetic field, and varies from ~0.1 R_E to 10 R_E, with the other two dimensions a factor 3–10 greater. The density structures are oriented with the longest sides in the general direction of the bow shock and magnetopause. Examples of density structures both convecting with the same velocity as the background magnetosheath flow ("embedded plasmoids"), and convecting with an excess x_{GSE} velocity component ("fast plasmoids") are found. Possible importance for the impulsive penetration mechanism for plasma entry in the magnetosphere is analyzed by comparing the results to laboratory results, via a parameter scaling. The estimation of the three-dimensional topology of the density enhancements will enable a comparison with localized magnetosheath populations inside the magnetosphere, observed earlier, to determine if these originate from penetrated magnetosheath density enhancements.

Citation: Karlsson, T., N. Brenning, H. Nilsson, J.-G. Trotignon, X. Vallières, and G. Facsko (2012), Localized density enhancements in the magnetosheath: Three-dimensional morphology and possible importance for impulsive penetration, *J. Geophys. Res.*, *117*, A03227, doi:10.1029/2011JA017059.

1. Introduction

[2] Plasma transport across the magnetopause from the magnetosheath into the magnetosphere is believed to be dominantly driven by reconnection during times of southwardly directed interplanetary magnetic field (IMF) [e.g., *Sibeck et al.*, 1999]. However, at times when IMF is northward, reconnection is absent from the dayside magnetopause, and other plasma transfer processes may dominate. Such processes include finite Larmor radius effects [e.g., *Stasiewicz*, 1993], diffusion processes [e.g., *Sibeck et al.*, 1999], Kelvin-Helmholtz vortices [e.g., *Hasegawa et al.*, 2004], and impulsive penetration [e.g., *Lemaire* 1977; *Lemaire and Roth*, 1991; *Echim and Lemaire*, 2000]. Probably several of these processes are active simultaneously with varying importance along the magnetopause; the Kelvin-Helmholtz vortices are, e.g., more likely to occur on the flanks than on the dayside magnetopause. It is an important task for magnetospheric physics to evaluate the relative importance and effectiveness of these mechanisms.

[3] The impulsive penetration (IP) mechanism postulates the preexistence of localized, coherent magnetosheath plasma structures with higher density than the surrounding magnetosheath plasma. In the IP theory, the excess momentum of these plasma structures allow them to cross the magnetopause, the position of which is determined by a pressure balance between the background magnetosheath plasma and the geomagnetic field. The exact mechanism for the penetration had not been agreed on, and unambiguous observational evidence of the IP mechanism is still lacking, although several observations of localized regions of magnetosheath plasma in the magnetosphere boundary layer, inside the dayside magnetosphere have been reported by *Lundin and Dubinin* [1984] and *Lundin et al.* [2003]. Indirect support for the IP theory comes from extensive observations in the laboratory of plasma clouds penetrating into regions of abruptly increasing magnetic fields [*Brenning et al.*, 2005, and references therein; *Echim and Lemaire*, 2000, and references therein.]

[4] The purpose of this paper is to take a first step in evaluating the IP theory by using Cluster multipoint measurements to establish the existence and three-dimensional properties of the postulated localized magnetosheath density

[1]Space and Plasma Physics, School of Electrical Engineering, Royal Institute of Technology, Stockholm, Sweden.
[2]Swedish Institute of Space Physics, Kiruna, Sweden.
[3]Laboratoire de Physique et Chimie de l'Environnement et de l'Espace, CNRS, Orléans, France.
[4]Earth Observation Unit, Finnish Meteorological Institute, Helsinki, Finland.
[5]Also at Geodetic and Geophysical Institute, Research Centre for Astronomy and Earth Sciences, Hungarian Academy of Sciences, Sopron, Hungary.

0148-0227/12/2011JA017059

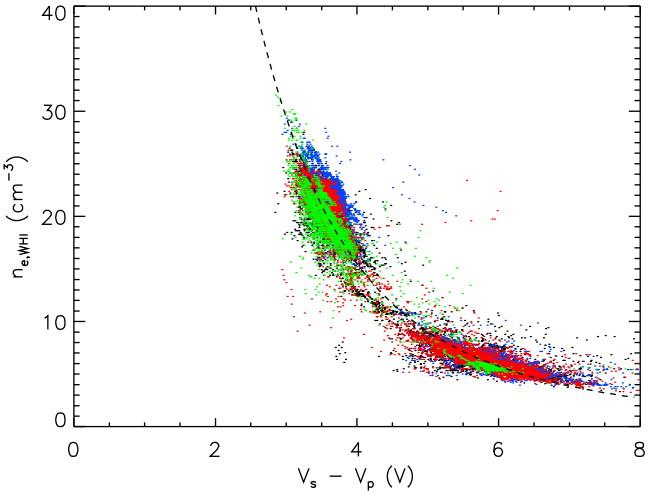

Figure 1. Electron density measured by WHISPER, as a function of the spacecraft potential for 6 January 2003. The color coding is as follows: black, S/C 1; red, S/C 2; green, S/C 3; blue, S/C 4. Indicated by the dashed line is the resulting fitted function (see text).

enhancements. Determining the three-dimensional morphology of such structures enables a comparison to laboratory experiments via parameter scaling [*Brenning et al.*, 2005]. Furthermore, when the properties of the magnetosheath density enhancements are known, a comparison with the boundary layer structures can establish if these structures are identical.

[5] Reports on possible localized density enhancements in the magnetosheath have been made by several authors. *Němeček et al.* [1998] used INTERBALL-1 and MAGION-4 data to observe 10 transient ion flux enhancements and estimated their dimension to be ~1 R_E (Earth radius). *Zastenker et al.* [2002] used several S/C to verify that such flux enhancements often convect with the magnetosheath flow. Magnetosheath pressure pulses have also been reported in connection with hot flow anomalies [*Omidi and Sibeck*, 2007; *Facskó et al.*, 2009], foreshock cavities [*Sibeck et al.*, 2002], and so-called transient density events [*Hubert and Harvey*, 2000]. Other observations of medium to large-scale density fluctuations have been interpreted as radial magnetosheath motion [*Sibeck and Gosling*, 1996, *Seon et al.*, 1999]. Recently jets of increased kinetic energy density have been reported by *Savin et al.* [2008] and *Amata et al.* [2011]. Finally, periodic density enhancements have been reported in connection with both magnetosonic waves [*Shevyrev et al.*, 2006] and magnetic mirror modes [e.g., *Constantinescu et al.*, 2003]. In the last study a three-dimensional morphology was estimated for one event.

2. Methodology

2.1. Instrumentation

[6] The four Cluster satellites were launched in 2000 in a polar orbit with a perigee of 4.0 R_E geocentric distance, and an apogee of 19.8 R_E. We use data from the following instruments: Electric Fields and Waves (EFW) for determining the electron density from the spacecraft potential [*Gustafsson et al.*, 1997], Cluster Ion Spectrometry (CIS) High Energy Analyzer (HIA) [*Rème et al.*, 2001], for the ion flow velocity and ion temperatures (available for S/C 1 and 3), and the Fluxgate Magnetometer (FGM) [*Balogh et al.*, 2001], for the DC magnetic field. For CIS HIA we only consider data from magnetospheric modes. We use spin resolution (4 s) data, which when measuring structures convecting with typical magnetosheath velocities corresponds to a spatial scale of a few ion gyro radii. Finally we use data from the Waves of High Frequency and Sounder for Probing of Electron Density by Relaxation (WHISPER) experiment [*Trotignon et al.*, 2003], for calibration of spacecraft potential density measurements.

2.2. Calibration of Density Measurements

[7] We use WHISPER data to calibrate the EFW spacecraft potential measurements in order to provide high time resolution, four-point measurements of the electron density. For event identification, we use a preliminary calibration (A. Vaivads, personal communication, 2009). Once a specific event is analyzed, we follow the method of *Escoubet et al.* [1997] and *Pedersen et al.* [2008], in that we establish a relation between the spacecraft potential with respect to the electric field probes, $V \equiv V_s - V_p$, where V_s is the potential of the outer surface of the spacecraft, and V_p is the probe potential, which is assumed to be close to the plasma potential in the dense magnetosheath plasma [*Pedersen et al.*, 2001]. For each event we fit data from the date in question using a least squares fit to the sum of two exponentials of the following form:

$$n_{e,WHI} = n_{e0} e^{-\frac{eV}{T_{e0}}} + n_{e1} e^{-\frac{eV}{T_{e1}}}, \quad (1)$$

where $n_{e,WHI}$ is the electron density determined by WHISPER, e is the elementary charge, and n_{e0}, n_{e1}, T_{e0}, and T_{e1} are free parameters. If more data is required, or data from the day in question is not available in the Cluster Active Archive, we use data from additional dates close to the event date. During the calibration process, we have not detected any systematic difference in the behavior between the spacecraft, and we have therefore only used one set of fitted parameters for all four spacecraft. Figure 1 shows an example of electron densities measured by WHISPER during 6 January 2003, as a function of the spacecraft potential. Indicated is the resulting fitted function, using the resulting fit values $n_{e0} = 29.2$ cm^{-3}, T_{e0}, $= 2.81$ eV, $n_{e1} = 137.8$ cm^{-3}, and $T_{e1} = 1.46$ eV. These are reasonable values of the fit parameters, comparable to the results of *Escoubet et al.* [1997]. For all calibrations, the resulting parameters had rather similar values to the example above.

[8] As a check that the calibration procedure has worked well, for 16 events the resulting density determinations using the spacecraft potential are compared to electron densities obtained from manual identification of the plasma resonances triggered by the active WHISPER sounding mode. Figure 2 shows such a comparison for an event from 5 January 2003, using the calibration parameters above.

2.3. Selection Criteria

[9] We have manually inspected orbits from the time periods given in Table 1. For these periods, the Cluster satellites spend an appreciable time in the magnetosheath per

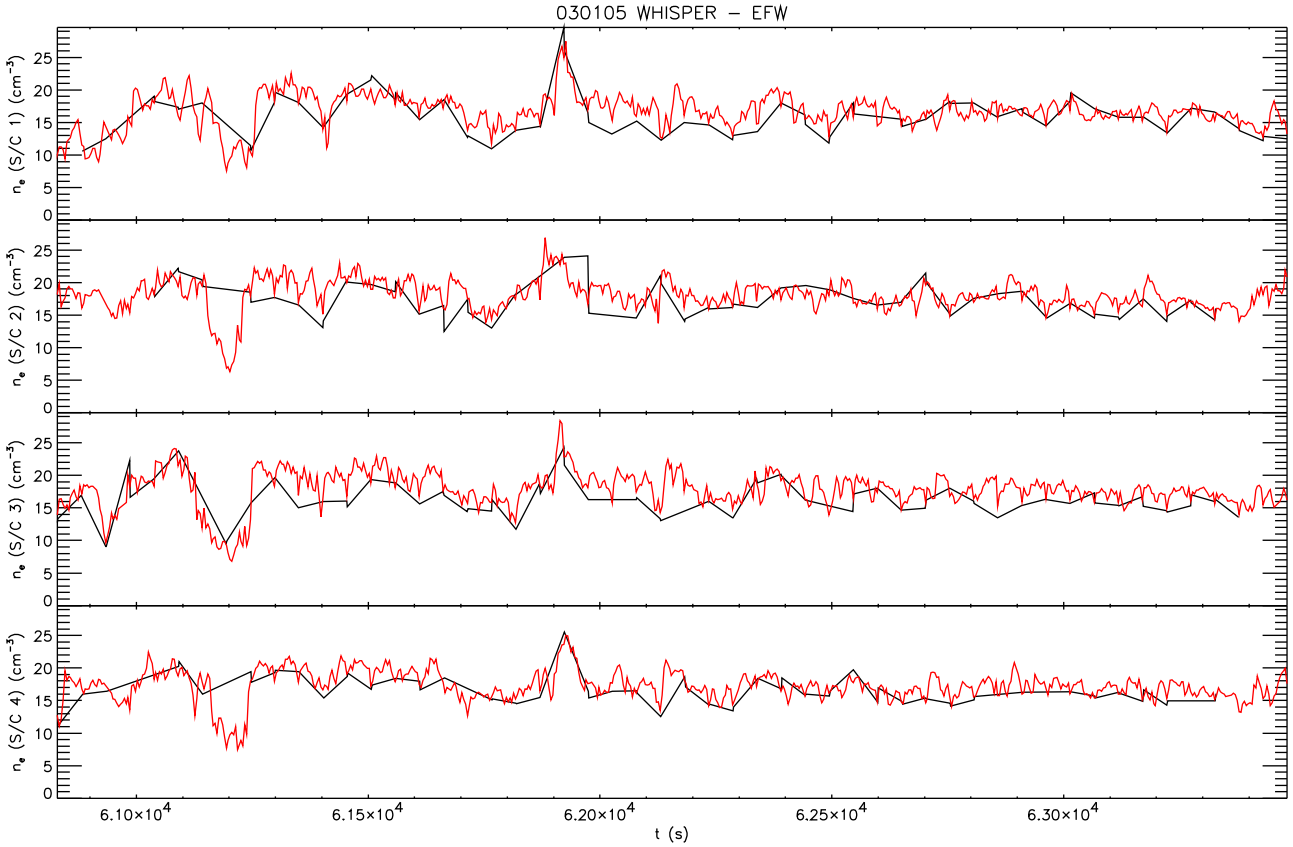

Figure 2. Density measurements from the calibrated spacecraft potential (shown in red) compared to electron densities obtained from manual identification of the plasma resonances triggered by the active WHISPER sounding mode (black), for a time period around one of the selected events at t = 61920 s, using the calibration parameters above. The time t is seconds from 00:00 UT on 5 January 2003.

orbit, and the satellite separations vary between approximately 0.5 and 2 Earth radii (R_E).

[10] *Lemaire* [1977] considers a density enhancement of 5% above the background density to be a typical value for a plasma density enhancement that might penetrate into the magnetosphere. However, in order to get clear and unambiguous results, we define a localized density enhancement as an increase of the electron density over the background density of at least 50% (using the preliminary calibration of the density measurements), where the background density is determined by a running boxcar average with a window width of 500 s. For a typical magnetosheath flow velocity of 200 km/s, this corresponds to a spatial scale of 16 Earth radii (R_E). We further use the following selection criteria to ensure that the measured density enhancements are really isolated, convecting structures, and not the signatures of either the magnetopause or the bow shock moving across the Cluster satellites, respectively, or by crossings of magnetopause surface wave structures:

[11] 1. We inspect Cluster Quicklook plots (see http://www.cluster.rl.ac.uk/csdsweb/) with particular emphasis on ion energy spectra, floating potential, and ion velocity. We only consider data temporally separated by at least 1 hour from any indication of a transition between magnetosheath and solar wind or magnetosphere, respectively.

[12] 2. We do not consider "nested structures," by which we mean the signature in, e.g., density that are observed by the Cluster satellites when the magnetopause passes them in first one direction, say outward, and then move back in the opposite direction. For such a magnetopause crossing, the satellite last observing the outward moving magnetopause would be the first to observe the inward crossing, and the other satellites would observe the inward crossing in the opposite order from the outward crossing. Similar nested structures can be observed at bow shock crossings, and by radial magnetosheath motion of the type reported by *Sibeck and Gosling* [1996].

[13] 3. The electron density values should be consistent with typical values of magnetosheath densities. *Phan et al.* [1994] give extrema of 5 and 95 cm^{-3} for magnetosheath electron density. The background electron density of our events vary between 4.1 and 42.5 cm^{-3}, which we consider as consistent with the values given by *Phan et al.* [1994].

[14] For the time intervals in Table 1 we have found 56 localized density enhancements fulfilling the above criteria. The event times and some other properties of these events, which will be described below, are given in Table 2.

Table 1. Time Periods Used in the Study

Start Date	End Date
13 Dec 2002	6 May 2003
1 Feb 2005	13 Apr 2005
14 Dec 2005	14 Jun 2006

Table 2. Details of Plasmoids Identified in the Cluster Data During the Time Periods Given in Table 1[a]

		S/C Position			Density		Minimum Variance Analysis		S/C Separation
Date	UT	x_{GSE} (R_E)	y_{GSE} (R_E)	z_{GSE} (R_E)	$n_{e,max}$ (cm^{-3})	$n_{e,max}$ / $n_{e,BG}$	$(\lambda_1/\lambda_2)_{av}$	α_{max} (°)	$\lvert\Delta r\rvert_{max}$ (R_E)
13 Dec 2002	00:42	0.8	16.1	4.1	14.5	2.60	4.3	22.3	0.76
15 Dec 2002	*22:44*	*5.0*	*18.4*	*−3.2*	*21.1*	*2.25*	*7.1*	*28.6*	*0.83*
16 Dec 2002	00:33	5.3	18.1	−4.2	17.1	1.80	1.7	51.4	0.94
16 Dec 2002	*12:38*	*6.0*	*11.3*	*−9.2*	*16.8*	*1.54*	*3.8*	*20.9*	*1.75*
17 Dec 2002	21:42	3.1	17.3	2.6	52.9	1.44	3.1	9.1	0.68
23 Dec 2002	10:01	8.0	14.6	−7.2	23.8	1.60	15.8	4.6	1.35
23 Dec 2002	10:12	8.0	14.4	−7.4	25.1	1.46	10.3	2.9	1.37
23 Dec 2002	10:55	7.9	14.1	−7.6	20.1	1.59	38.5	4.0	1.42
23 Dec 2002	13:43	7.7	12.1	−8.6	30.7	1.77	3.1	8.3	1.61
23 Dec 2002	15:21	7.5	10.8	−9.1	24.9	1.56	3.2	18.0	1.71
23 Dec 2002	16:26	7.3	9.9	−9.4	24.4	1.43	2.2	33.1	1.78
27 Dec 2002	01:17	1.8	11.0	6.7	54.1	1.72	44.4	3.8	0.84
27 Dec 2002	01:33	2.0	11.3	6.6	46.4	1.53	10.5	15.6	0.84
27 Dec 2002	*01:58*	*2.2*	*11.7*	*6.5*	*46.1*	*1.60*	*1.3*	*154.0*	*0.84*
27 Dec 2002	*02:14*	*2.3*	*11.9*	*6.4*	*42.8*	*1.50*	*3.9*	*12.0*	*0.84*
2 Jan 2003	*03:52*	*9.1*	*9.3*	*−9.2*	*35.3*	*1.45*	*2.9*	*37.1*	*1.72*
5 Jan 2003	17:12	−0.5	13.3	5.8	27.0	1.51	1.8	57.0	0.81
10 Jan 2003	08:48	5.2	11.0	6.4	44.4	1.37	15.8	7.4	0.83
10 Jan 2003	09:43	6.0	11.7	5.9	42.7	1.39	7.8	3.7	0.83
9 Feb 2003	10:33	8.2	−0.8	−9.8	26.8	1.50	8.7	6.9	2.04
24 Feb 2003	*11:40*	*9.1*	*3.9*	*6.8*	*15.6*	*1.44*	*4.6*	*25.1*	*0.82*
24 Feb 2003	13:08	10.9	3.9	6.3	15.4	1.55	1.9	60.6	0.82
7 Mar 2003	13:06	9.0	−4.5	−9.9	24.7	1.71	4.2	136.0	1.96
7 Mar 2003	17:30	8.5	−4.5	−9.9	22.7	1.58	3.5	17.8	1.99
1 Apr 2003	*06:43*	*12.0*	*−3.9*	*5.7*	*36.4*	*2.63*	*1.4*	*101.7*	*0.81*
7 Apr 2003	12:39	4.3	−7.7	−10.0	58.4	1.40	4.6	17.4	2.04
7 Apr 2003	13:28	3.5	−7.1	−9.7	58.8	1.40	3.2	15.7	2.08
1 May 2003	04:16	2.9	−11.7	−9.9	32.8	1.73	1.5	51.9	1.85
1 May 2003	04:36	−1.0	−10.2	−9.9	33.4	1.88	2.6	54.6	1.87
6 May 2003	00:42	0.9	−10.0	−10.1	60.6	1.87	8.3	10.7	1.98
6 May 2003	00:47	0.8	−9.9	−10.1	49.8	1.67	2.2	94.4	1.99
6 May 2003	01:45	0.3	−8.9	−10.0	46.6	1.61	2.7	43.5	2.04
4 Feb 2005	*07:44*	*11.7*	*8.8*	*3.4*	*19.5*	*1.70*	*1.5*	*57.7*	*0.21*
8 Feb 2005	*22:02*	*8.8*	*7.0*	*5.3*	*21.3*	*2.07*	*2.1*	*57.9*	*0.23*
13 Feb 2005	*16:38*	*9.8*	*6.3*	*5.1*	*38.4*	*1.37*	*3.9*	*29.4*	*0.22*
13 Feb 2005	*16:45*	*9.9*	*6.3*	*5.0*	*38.3*	*1.37*	*2.0*	*37.1*	*0.22*
8 Apr 2005	08:50	7.6	−10.1	−10.7	24.8	1.59	1.5	78.0	0.35
8 Apr 2005	09:10	7.3	−10.0	−10.8	22.9	1.58	1.8	15.1	0.36
8 Apr 2005	*09:43*	*6.9*	*−9.8*	*−10.8*	*19.5*	*1.68*	*13.2*	*14.6*	*0.37*
10 Apr 2005	22:57	3.1	−7.7	−10.7	48.8	1.78	3.7	11.3	0.49
13 Apr 2005	*08:19*	*2.5*	*−7.6*	*−10.6*	*40.6*	*2.34*	*6.4*	*28.8*	*0.50*
19 Dec 2005	20:55	6.4	6.1	−11.7	50.0	1.38	4.8	16.2	1.44
19 Dec 2005	22:54	5.9	4.1	−11.3	51.0	1.37	5.1	24.4	1.70
29 Jan 2006	*06:56*	*9.5*	*0.7*	*−11.8*	*11.8*	*1.48*	*2.2*	*48.2*	*1.49*
2 Mar 2006	05:24	12.7	3.2	2.9	43.9	2.18	4.0	20.6	1.53
10 Mar 2006	*23:18*	*1.9*	*−4.9*	*−10.1*	*63.2*	*1.98*	*5.7*	*16.9*	*1.57*
13 Mar 2006	06:30	3.9	−5.5	−11.1	17.4	1.36	4.6	21.4	1.37
22 Mar 2006	17:40	4.2	−6.6	−11.5	12.4	1.80	3.4	4.1	1.37
22 Mar 2006	*17:58*	*3.9*	*−6.4*	*−11.4*	*17.4*	*2.52*	*5.4*	*23.5*	*1.33*
22 Apr 2006	13:34	2.1	−9.7	−11.9	30.0	2.07	4.9	22.2	1.65
22 Apr 2006	14:53	1.2	−8.8	−11.8	24.6	1.89	6.9	38.4	1.54
6 May 2006	23:26	−1.8	−7.1	−11.3	26.1	1.49	9.1	20.5	1.39
3 Jun 2006	20:55	−2.5	−16.9	−9.5	8.7	2.13	3.2	30.2	1.95
4 Jun 2006	03:38	−4.0	−13.5	−11.6	11.9	1.8	9.1	20.7	1.69
8 Jun 2006	17:26	−4.3	−15.7	−10.3	16.3	1.96	3.1	18.9	1.78
11 Jun 2006	00:58	−4.6	−16.2	−9.8	9.9	1.55	10.4	3.9	1.77

[a]The columns denote, from left to right, date and universal time for the detections, spacecraft position in the Geocentric Solar Ecliptic (GSE) coordinate system, maximum density $n_{e,max}$, and ratio of maximum density and magnetosheath background density, $n_{e,max}$ / $n_{e,BG}$, average ratio of eigenvalues for minimum and medium variations $(\lambda_1/\lambda_2)_{av}$, maximum angle between minimum variance normal between spacecraft, α_{max}, and maximum spacecraft separation, $\lvert\Delta r\rvert_{max}$. Entries in italics are classified as "fast" plasmoids (see section 3.1).

2.4. Minimum Variance Analysis

[15] Manual inspection showed that for all events, the density enhancements were associated with a clear magnetic field variation. (We shall therefore from now on alternatively refer to the density enhancements as "plasmoids," following the definition of *Bostick* [1956]: "plasma-magnetic entity," not necessarily with a toroidal geometry.) Examples of this are shown in Figure 3, where the ratio of electron density to background electron density (denoted as $n_e/n_{e,av}$ in Figure 3)

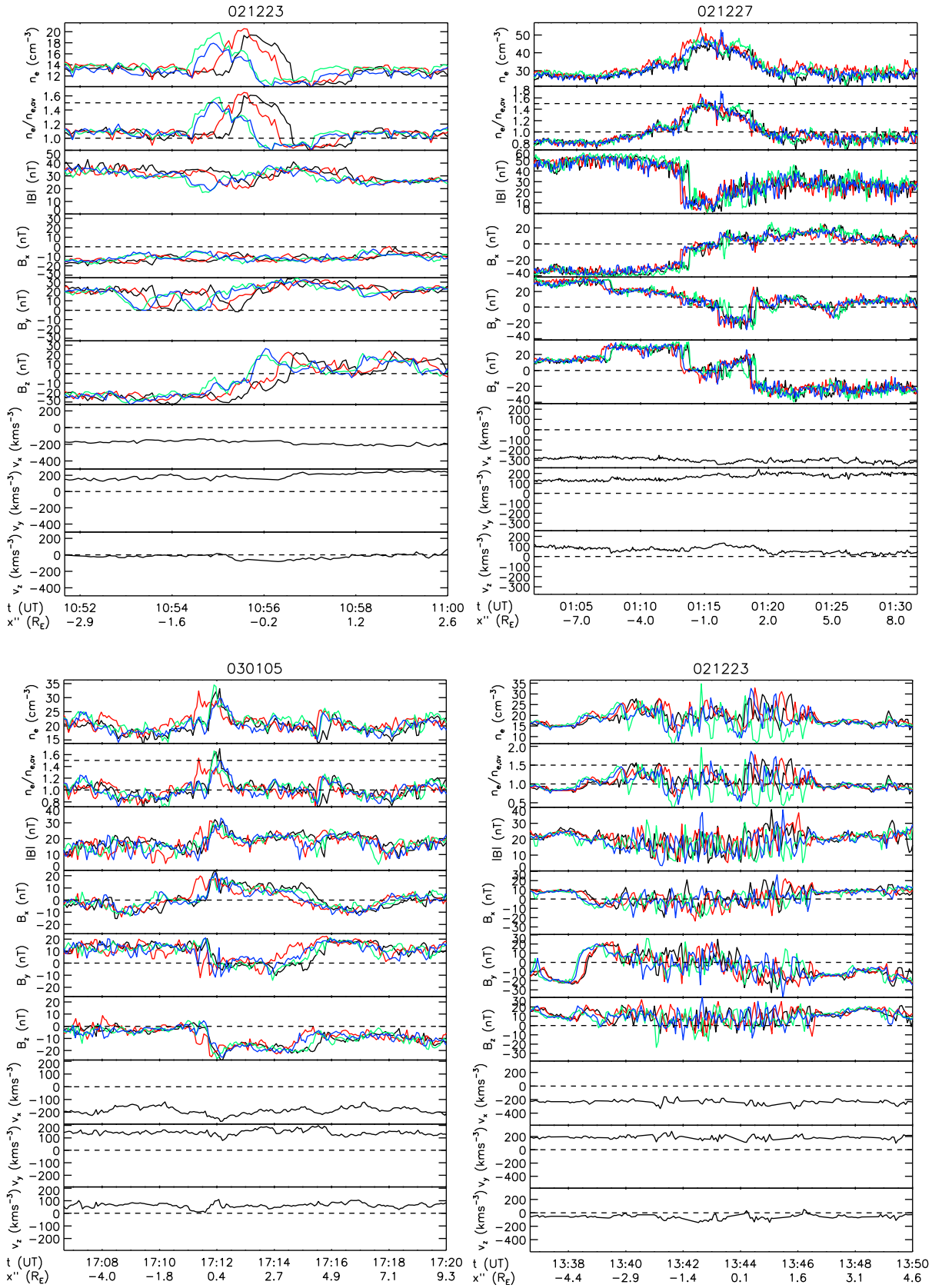

Figure 3. Cluster data from four encounters of density enhancements. From top to bottom the panels show electron density, ratio of electron density to background density, total magnetic field, the three components of the magnetic field in GSE coordinates, and the three components of the drift velocity in GSE coordinates. The color coding is the same as in Figure 1. For the velocity only the data from S/C 1 is shown.

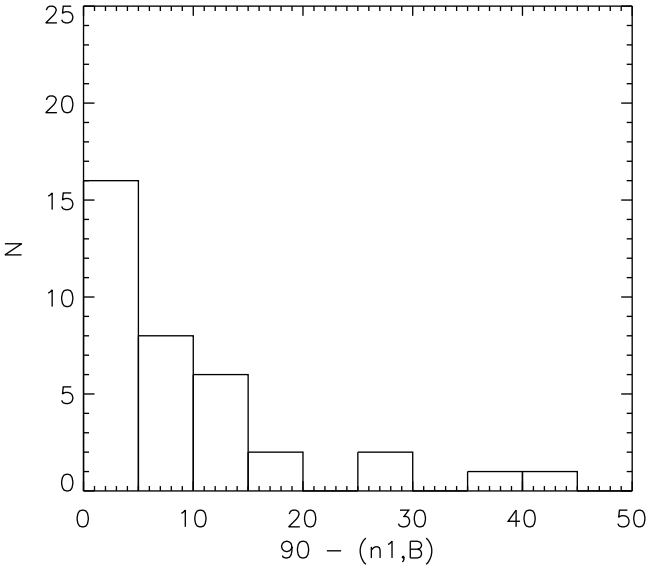

Figure 4. Histogram of number of events versus the deviation from 90° in the angle between the minimum variance normal $\hat{\mathbf{n}}_1$ and the background magnetic field.

magnetic fields (**B**) and ion velocity (**v**) for four different events are plotted. For all plots the Geocentric Solar Ecliptic (GSE) coordinate system is used. Note the virtually unchanged ion drift velocity. The first three events are examples of the isolated density enhancements that make up the majority of the cases studied here, whereas the last one is one example out of two events, with large-amplitude quasi-periodic variations included in this study.

[16] We have performed a minimum variance analysis (MVA) [*Sonnerup and Cahill*, 1967] of the magnetic field for each event. The MVA method is an established tool for determining the orientation of large-scale boundaries, current layers, discontinuities and other transition layers in a plasma [*Sonnerup and Scheible*, 1998].

[17] We have applied MVA over the whole event, plus a small region outside it. The robustness of the result has been checked by varying the interval slightly. This is a standard procedure in analyzing magnetic clouds in the solar wind [e.g., *Klein and Burlaga*, 1982; *Bothmer and Schwenn*, 1998; *Echer*, 2006]. It is also standard procedure in auroral physics, when determining the orientation of field-aligned current sheets. The result of the MVA is a set of three eigenvectors for each event, giving the directions of minimum, medium and maximum variance, respectively, with the minimum variance direction indicating the normal to the plane of the magnetic field discontinuity. The eigenvalues associated with each eigenvector allows for an estimate of the quality of the eigenvector determination; the eigenvalues should be well separated.

[18] In the below estimates of scale sizes, we have discriminated between cases with a value of at least 3 for the ratio between the eigenvalues associated with the minimum and medium variance eigenvectors, and cases with a smaller ratio (which we denote as "degenerate"). A consideration of this ratio is a common criterion for an acceptable eigenvector determination (a minimum ratio of 2 was recommended in a study of errors in MVA by *Lepping and Behannon* [1980]). For a clear separation of eigenvalues, the minimum variance direction, $\hat{\mathbf{n}}_1$, identifies the shortest dimension of the three-dimensional structure associated with the magnetic field variations.

[19] We also take note of events with an angle between the MVA eigenvectors $\hat{\mathbf{n}}_1$ for the different spacecraft (denoted by α_{max}) greater than 30°. Such events have a surface with a curvature which is not negligible on the spacecraft separation scale.

[20] In Figure 4 we show the distribution of the angle between the MVA normal vector, and the background magnetic field, defined as the mean of the magnetic field in a window with a width of 400 s centered on the maximum density of the event. The average is taken over all four S/C, excluding cases which are degenerate, or have $\alpha_{max} > 30°$. It can be seen that for a majority of these cases, this angle is close to 90°. We now proceed to make a coordinate transformation from the GSE coordinate system to a system where $\hat{\mathbf{x}}'$ is directed along $\hat{\mathbf{n}}_1$, $\hat{\mathbf{z}}'$ is directed along the projection of **B** in the plane perpendicular to $\hat{\mathbf{n}}_1$, and $\hat{\mathbf{y}}'$ completes the right-handed system. The orientations are shown in the conceptual sketch of Figure 5a. We determine $\hat{\mathbf{n}}_1$ for all S/C crossing the structure, and for nondegenerate events

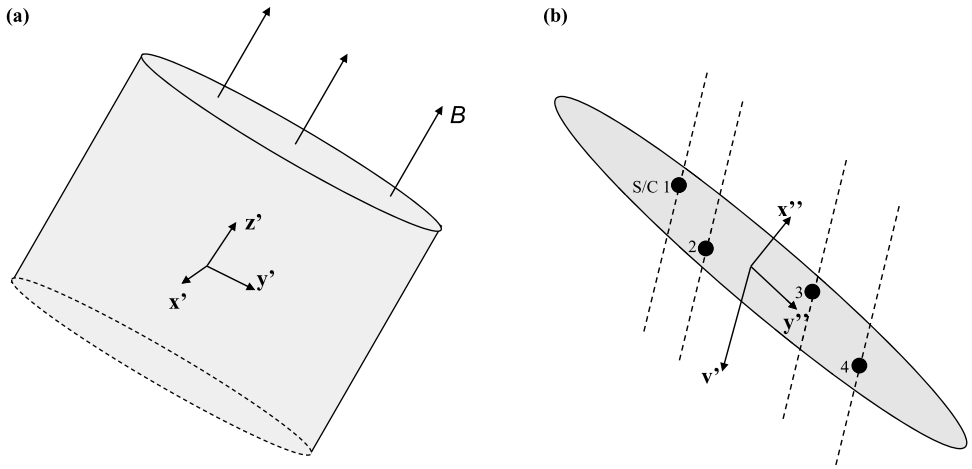

Figure 5. (a) Schematic representation of coordinate system used in minimum variance analysis. (b) Schematic of the probing of the plasmoid as is sweeps across the spacecraft.

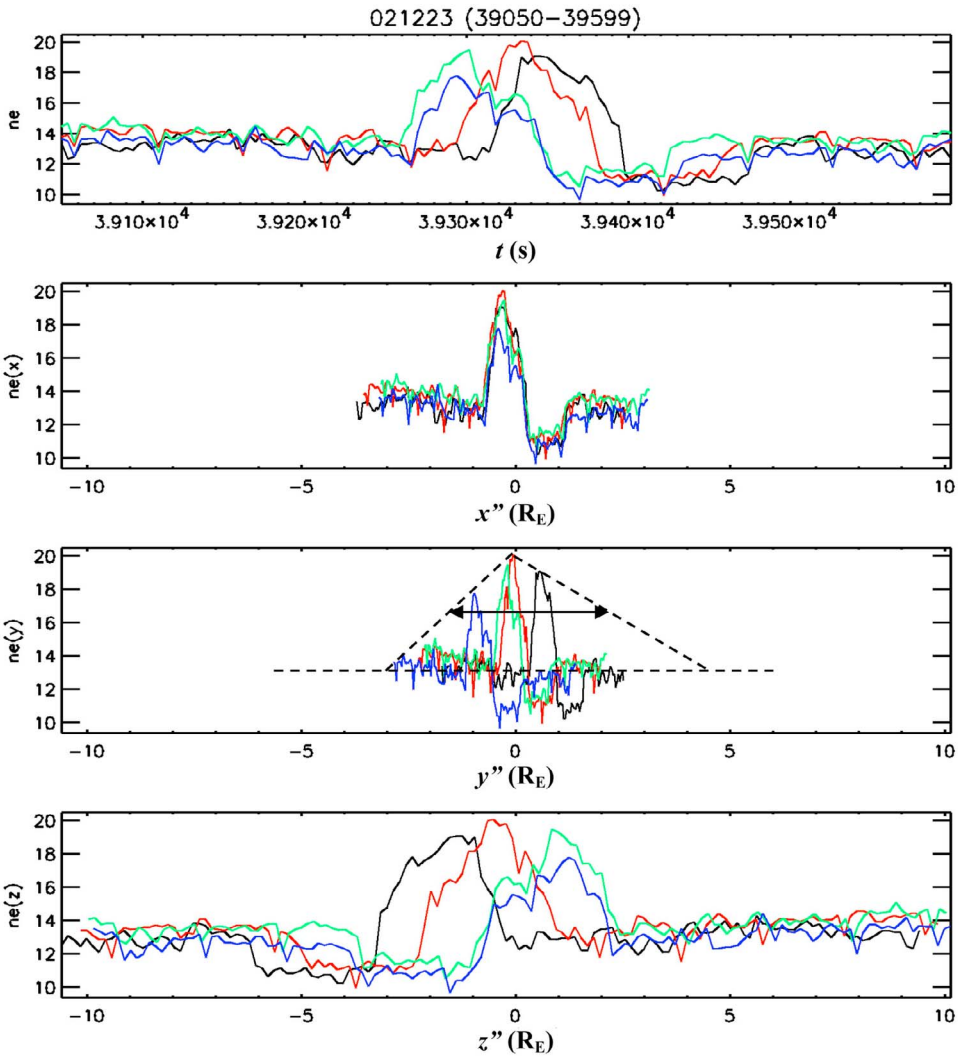

Figure 6. The top panel shows the density data as time series. The x axis shows seconds from 00:00 UT, 23 December 2002. The next three panels show the density as a function of the three coordinates, x'', y'', and z''. The color coding is the same as in Figure 1. In the third panel an example is seen of the interpolation of the density variation in this direction. From this interpolation the FWHM is determined and used as an estimate of the scale size in this direction. In the last panel can be seen an example of inconsistent density variations.

where the difference between any normal is less than 30°, we use the normal calculated from data from S/C 1 if it is available, otherwise from S/C 2 (no events are observed by only two S/C). For degenerate cases, and when $\alpha_{max} > 30°$, we use the normal calculated for the spacecraft which measures the highest maximum density.

[21] After determining the normal $\hat{\mathbf{n}}_1$, we move into the plasma frame of motion by the further coordinate transformation

$$x'' = x' - v'_x \Delta t,$$
$$y'' = y' - v'_y \Delta t,$$
$$z'' = z' - v'_z \Delta t,$$

where the vector $\mathbf{v}'$ is the magnetosheath plasma flow, normally determined by averaging the HIA velocity (in GSE) of S/C 1 over a period of 200 s around the maximum electron density of the event, and transformed into the primed system. As will be discussed in section 3.1, a majority of the plasmoids have the same velocity as the surrounding magnetosheath plasma, whereas about one fourth of them are associated with a higher velocity than the surrounding medium. For the latter, a 12 s average around the maximum velocity associated with the plasmoid was used. The origin of the double-primed system is determined by setting the primed coordinates to zero at the position of S/C 3 at an arbitrary reference time [c.f. *De Keyser et al.*, 2004]. Δt denotes the distance in time from this reference time. The coordinate system is illustrated in the conceptual Figure 5b. If the density enhancements are moving with the velocity $\mathbf{v}'$, they should now line up along x''. As an example of this procedure, we show the results of its application on the first event shown in Figure 3. In Figure 6 we thus show the density as a function of time and of x'', y'', and z''. As expected the

Table 3. Symbols Used for Data Points in Figure 5.

Method Number	Description	Plot Symbol
1a	double extrapolation in one direction, with inconsistency in the other direction	solid circle
1b	single extrapolation in one direction, with inconsistency in the other direction	diamond
2	S/C separation along "inconsistent" direction; lower limit	open square
3	extrapolation in both directions	solid square
4a	size of region probed without any variation in n_e; lower limit	open triangle, pointing upward
4b	same as Method 4a, but for degenerate cases, and for $\alpha_{max} > 30°$	open triangle, pointing downward
5	cross-correlation for quasiperiodic structures	open circle

density profiles from the four spacecraft clearly line up when plotted against x''.

2.5. Scale Sizes

[22] Although the density profiles line up in the second panel, they do not have the same maximum value. This can be interpreted as a spatial variation along the y'' and z'' directions, as the spacecraft sample different regions of the structure when it moves across the spacecraft constellation, as illustrated in Figure 5b. This will be used to make an estimate of the 3D topology of the structures.

[23] First, the scale size of the structure in the x'' direction can be conveniently defined as the full width at half maximum (FWHM) of the density profile with the highest maximum (in Figure 6 that will be the profile for S/C 2), where we set the zero level at the background density around the structure.

[24] For the scale sizes in the other two directions we can now make some estimates by the following methods: If the variation along, e.g., y'' of the maximum value of the density profiles for each spacecraft is consistent with the decrease from some maximum density along that direction, whereas no such consistent behavior is seen in z'', we take this as a strong indication that the scale length of the structure is appreciably longer in the z'' direction, than in the y'' direction. The scale size in the y'' direction can now be estimated by extrapolation, and subsequent determination of the FWHM, as illustrated in Figure 6. For the scale size along z'', we can get a lower limit by taking the size of the region probed in the z'' direction (defined as the separation between the points where the two most separated spacecraft where the density increase drops to half the maximum value). We will call this method of estimating the scale sizes Method 1a for the scale size along y'', and Method 2 for the "inconsistent" direction along z''. For some events it is only possible to do the extrapolation along y'' in one direction from the maximum, which then provides a lower limit of the scale size. (This will be called Method 1b.) The roles of y'' and z'' may of course be reversed. For some other events, the variations are consistent with a density decrease along both y''

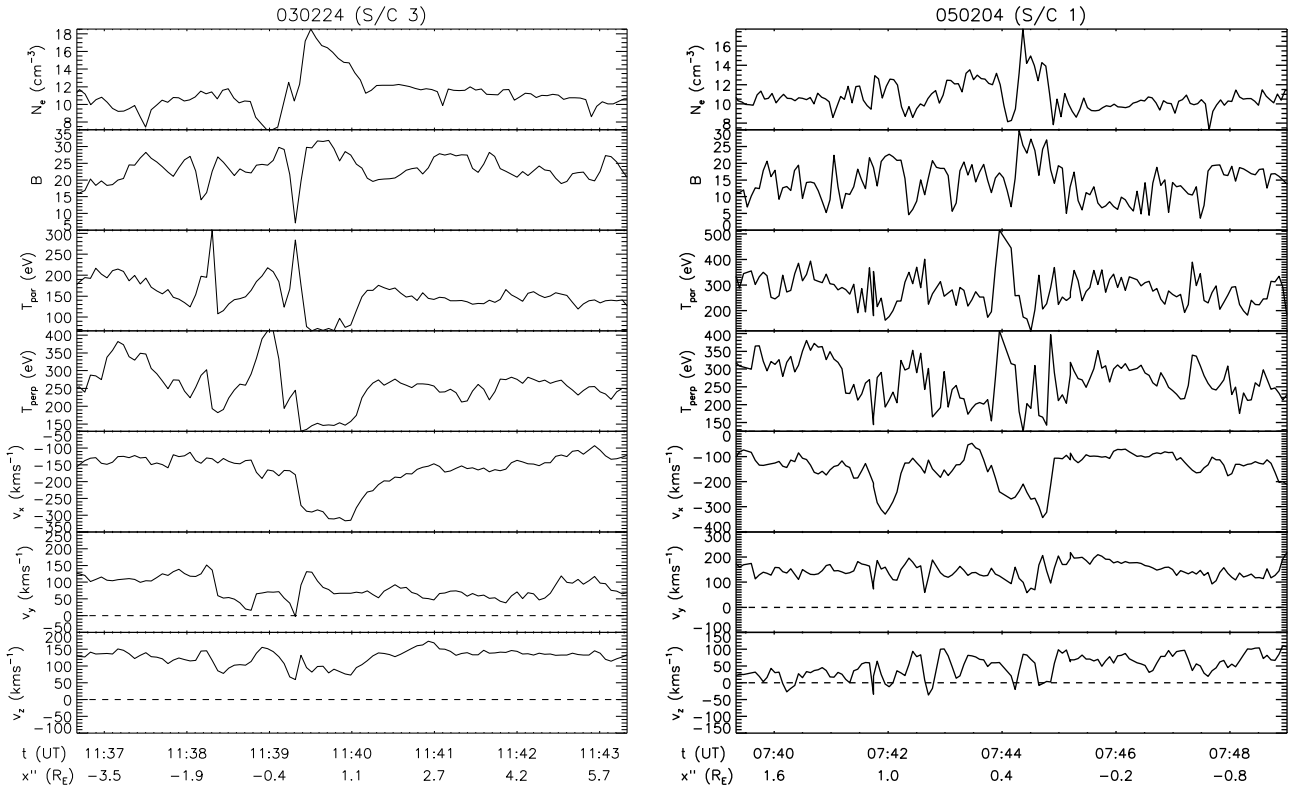

Figure 7. Two examples of plasmoids with clearly higher velocity than the surrounding magnetosheath plasma. From top to bottom, the panels show electron density, total magnetic field, parallel (to **B**), and perpendicular temperatures, and the three components of the velocity in GSE coordinates.

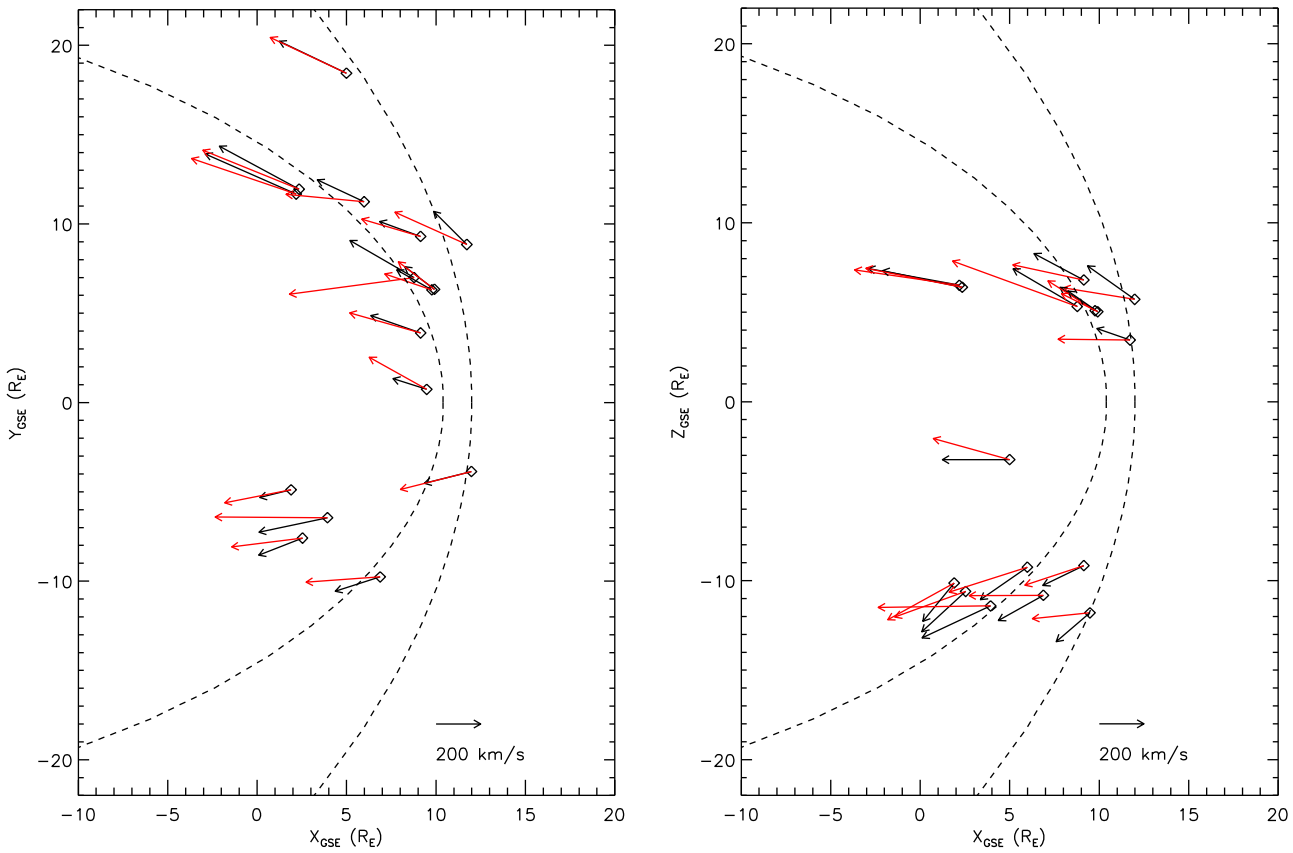

Figure 8. Position of and velocities projected onto the *xy* and *xz* GSE planes, for the 16 fast plasmoids. The black vectors show the background velocity, and the red vectors the plasmoid velocity.

and z''. We still use extrapolation and determination of the FWHM as an estimate of the scale sizes, but this is of course a more uncertain estimate (Method 3). For other events, such as that from 27 December 2002 in Figure 3, there is essentially no variation in maximum electron density between the spacecraft. The size of the region probed in the y'' and z'' directions (similar to Method 2) then provides a lower limit of the scale size (Method 4a). For degenerate cases and cases for which $\alpha_{max} > 30°$, we proceed as in Method 4a, using the spacecraft which measures the highest maximum density for the MVA. We call this Method 4b. Finally, for two cases, the density enhancements are associated with quasiperiodic oscillations in the density; an example is seen from 23 December 2002 in Figure 3. For these two cases we construct the cross-correlation between pairs of S/C. For S/C pairs with a smaller correlation coefficient than 0.5 we use the S/C separation along y'' and z'' as an upper limit of the scale sizes in these directions. The lowest such estimate along each direction is used as the final estimate (Method 5). For one case the correlation coefficient was greater than 0.5 for all S/C combinations. In that case the largest spacecraft separation in each direction was used as the estimate of the scale size.

[25] With only four measurement points there are of course some uncertainties in the estimates of the scale sizes. The greatest uncertainties are associated with only establishing a lower limit of the scale size. Such measurements are represented with unfilled symbols in Figure 9. Furthermore the assumption of a linear decrease of the density from the maximum is somewhat arbitrary, but nevertheless these estimates represent a major step forward from single spacecraft measurements. A summary of the methods used, and the corresponding plotting symbols used in section 3, are given in Table 3. Starting from section 3, we drop the double primes from the coordinates.

3. Results

3.1. Velocity of Plasmoids

[26] One question that appears when considering plasmoids convecting with the surrounding magnetosheath flow is if this type of density enhancements will actually reach the magnetopause, or just sweep by it, following the tangential magnetosheath flow. We have however also encountered plasmoids with a local velocity different from that of the surrounding magnetosheath plasma. We have identified 16 plasmoids with a greater than 50% density enhancement, and a local velocity where the GSE *x* component shows at least a 10% increase over that of the surrounding magnetosheath flow. Two such plasmoids are shown in Figure 7. We will denote these plasmoid as "fast plasmoids," whereas the remaining ones will be denoted as "embedded plasmoids." For the event from 24 February 2003, a density enhancement with its maximum encountered by S/C 3 at approximately 11:39:30 UT is seen to be associated with a large increase (by about a factor of two) in the (negative) GSE *x* component of the velocity. In front of the plasmoid an increase in both the parallel and perpendicular temperatures can be seen as an indication that the surrounding

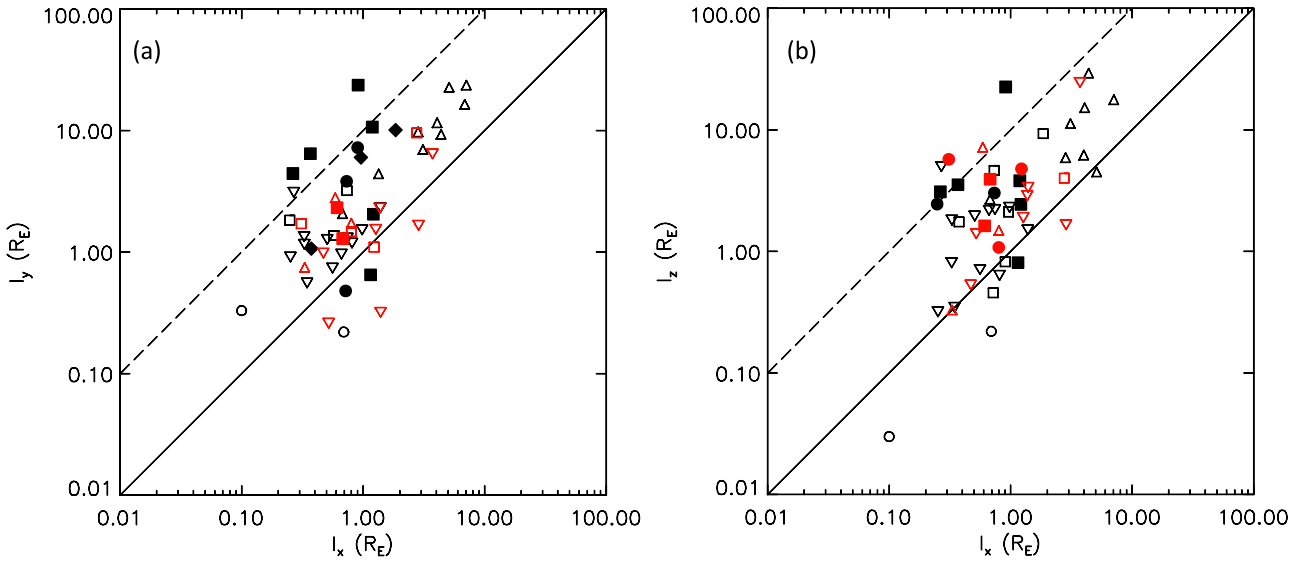

Figure 9. Estimated scale sizes l_x, l_y, and l_z. Black symbols represent embedded plasmoids, and red symbols fast plasmoids.

magnetosheath plasma is disturbed by the plasmoid, as it makes its way through the surrounding medium. Similarly, the plasmoid encountered by S/C 1 on 4 February 2005 at close to 07:45 UT is associated with a factor of around three increase of the velocity in the GSE x direction, and a temperature increase in front of it.

[27] The velocities of the 16 fast plasmoids are plotted as red arrows in the GSE xy and xz projections in Figure 8, together with their corresponding background flow velocities in black. There is a tendency for the plasmoids to have a larger velocity than the background magnetosheath flow velocity, and to be directed more in the GSE x direction. We

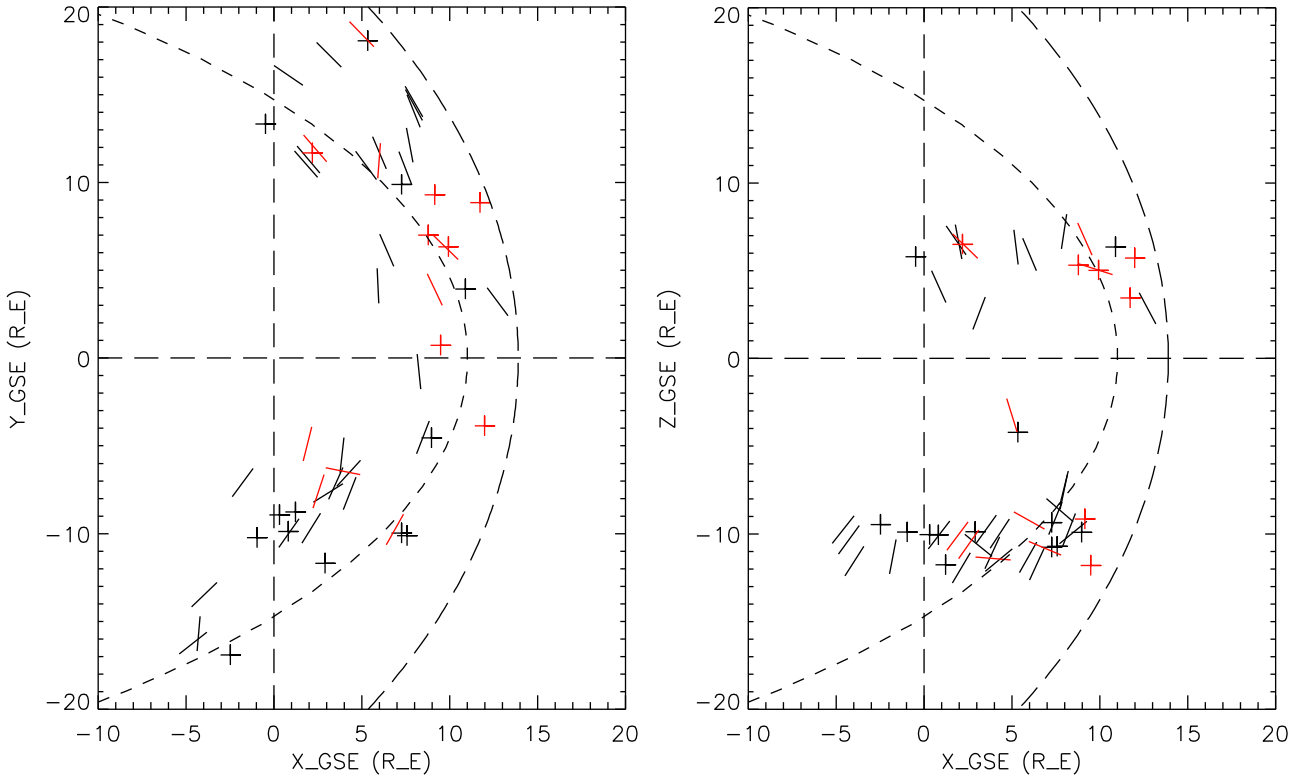

Figure 10. Location and orientation of plasmoids, illustrated by plotting the projection of the plane perpendicular to the minimum variance normal onto the xy and xz GSE plane, respectively, for nondegenerate events with $\alpha_{max} > 30°$. The location of the remaining events are plotted as crosses. The same color coding as in Figure 9 is used.

interpret this as an effect of the increased inertia of the plasmoids due to their increased density. Even if they are originally convecting together with the surrounding magnetosheath plasma, as they feel the same acceleration as the surrounding medium, which produces the smooth, tangential magnetosheath flow close to the magnetopause, the plasmoids will still have a considerable velocity component normal to the magnetopause surface. The velocity increases in Figure 8 suggest that this velocity component will be of the same order as the background flow.

3.2. Scale Sizes

[28] In Figures 9a and 9b, we show the shortest scale size (l_x) versus the estimated scale sizes in the y and z directions, denoted by l_y and l_z, respectively. Embedded plasmoids are plotted in black, whereas fast plasmoids are plotted in red. The solid line corresponds to the line $l_x = l_y$, and the dashed line to $l_x = 10l_y$. It can be seen that for most events l_y and l_z are a factor 1–10 greater than l_x, consistent with the determination of the direction of x by MVA. For plasmoids where l_y has been determined by Method 1a, it is very likely that they have their longest extension along the magnetic field direction. They can be visualized as flux tubes, flattened in one of the directions perpendicular to **B**. However, from Figure 9b, it is also clear that for two of the events, we have a strong indication that it has a shorter extension along **B**, than in the perpendicular (to **B**) direction y.

3.3. Orientation and Location

[29] In Figure 10 we show the location and orientation of the plasmoids, by plotting the projection of the plane perpendicular to the normal $\hat{\mathbf{n}}_1$ in the GSE xy- and xz planes, for the nondegenerate cases with $\alpha_{\max} > 30^\circ$. For reference also the location of the remaining events are plotted as crosses. Again embedded and fast plasmoids are plotted in black and red, respectively. Also indicated are the statistical positions of the magnetopause for moderate solar wind pressure [*Sibeck et al.*, 1991], and the magnetosheath [*Burgess*, 1995]. We note a clear tendency for the structures to orient themselves in the general direction of the magnetopause or bow shock. In section 4 we will discuss possible implications for the generation mechanism for these structures, and for possible impulsive penetration.

4. Discussion and Conclusions

[30] This investigation has shown the existence of localized density enhancements of over 50% and even over 100% with scale sizes of the order of 0.1–10 R_E. These density enhancements, or plasmoids, have one dimension which is appreciably shorter than the others and directed perpendicular to the background magnetic field, and thus take the form of flattened flux tubes. There seems to be no systematic difference in either the scale sizes or the orientations of embedded and fast plasmoids. The fact that their orientation is such that the normal to the shortest direction tends to be parallel to the magnetopause normal, as seen in Figure 10, has some importance of the potential impulsive penetration into the magnetosphere. An analysis of laboratory experiments of plasmoid penetration across abrupt magnetic barriers, by *Brenning et al.* [2005], shows that the penetration or otherwise, as well as the penetration mechanism can be predicted by the plasmoid's position in a parameter space (β_k,w'). Here β_k is the kinetic beta: $\beta_k = W_K/W_B$, with the kinetic energy density of the plasmoid $W_K = n_e m_i v^2$, and the magnetic energy density $W_B = B_0^2/2\mu_0$, which is to be evaluated at the region into which the plasma is trying to penetrate, i.e., in our case just inside the magnetopause. w' is a normalized width, $w' = \left(w/r_{gi}\right)K\sqrt{W_{i,th}/W_B}$. Here w is the dimension of the plasmoid, in the direction tangential to the magnetic barrier, r_{gi} is the ion gyro radius evaluated with the flow velocity, and the magnetospheric magnetic field: $r_{gi} = (m_i v)/(eB_0)$, $W_{i,th}$ is the ion thermal energy density; $W_{i,th} = (n_i m_i v_{i,th}^2)/2$, where $v_{i,th}$ is the ion thermal velocity, and K is a numerical factor, determined experimentally, $K \approx 2.3$. Any quantities not defined above, have their usual meanings. Combining experimental results and theoretical energy considerations, *Brenning et al.* [2005] determined boundaries in parameter space for regions of plasmoid rejection, and penetration by *magnetic expulsion* via diamagnetic currents or *self-polarization*, where an electric field $\mathbf{E} = -\mathbf{v} \times \mathbf{B}$ is set up within the plasmoid [*Wessel et al.*, 1988; *Echim and Lemaire*, 2000; *Brenning et al.*, 2005]. We now try to place the plasmoids of this study into this parameter space by estimating β_k and w'. For simplicity we use typical values for magnetosheath and magnetospheric quantities: $B_0 = 50$ nT, and a value of the ion temperature $T_i = 3.3 \times 10^6$K (= 284 eV), which is an average temperature for the near-magnetopause magnetosheath [*Phan et al.*, 1994], has been used to evaluate $W_{i,th}$. Figure 11 shows the result of these estimates, with the diamond data points corresponding to using the maximum scale size of the plasmoid for w, which should be the most appropriate measure, since the plasmoids tend to align themselves in the general orientation of the magnetosphere, as seen in Figure 10. For comparison data points marked by pluses, indicate a calculation using the smallest value of the scale size, which usually is l_x. For the drift velocity we use the measured values for the plasmoids. It is clear that this velocity in many cases will be tangential to the magnetopause, but as showed in section 3.1 the residual velocity of plasmoids can be as large as, or even larger than the background magnetosheath flow velocity.

[31] We see that a majority of the plasmoids end up in the magnetic expulsion region, which shows that according to the scaling laws determined by *Brenning et al.* [2005] these plasmoids have the potential to penetrate into the magnetosphere. Here the size of the plasmoid results in a time scale for the diffusion of the magnetospheric magnetic field into the plasmoid which is greater than the time scale of the actual penetration. The reason for this is that the diamagnetic currents on such large-scale plasmoids are not strong enough to trigger the instabilities responsible for the fast magnetic diffusion [*Hurtig et al.*, 2005; *Brenning et al.*, 2005]. For a three-dimensional plasmoid the penetration by magnetic expulsion may be associated with localized reconnection, as the plasmoids deform the magnetopause magnetic field, locally creating regions of antiparallel magnetic fields [*Ma et al.*, 1991]. We have here neglected the fact that the plasmoids have a nonzero magnetic field in the magnetosheath, something that may affect the boundary between the regions of magnetic expulsion, and self-polarization. Furthermore, if the plasmoid penetrates, after a while magnetic field diffusion will take place, and

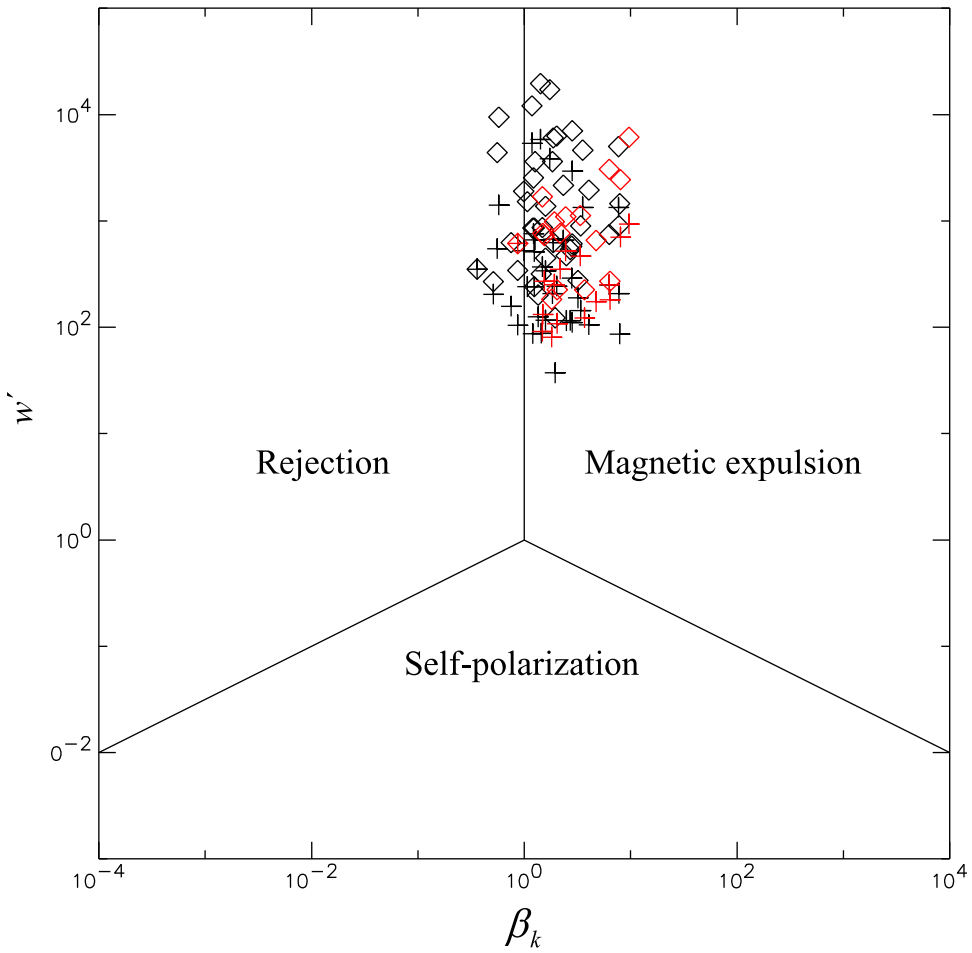

Figure 11. Plasmoid parameters in the parameter space defined by *Brenning et al.* [2005]. *w'* is a normalized width of the plasmoid (see text for definition), and β_k is the kinetic beta, evaluated with the directed velocity of the plasmoid, and with the magnetic field inside the magnetosphere. The mechanisms of the different regions pertain to the situation of penetration at the boundary of the high magnetic field region. See also text for explanation of symbols. The same color coding as in Figure 9 is used.

the plasmoid can make the transition to a self-polarized state.

[32] Final experimental verification of impulsive penetration into the magnetosphere is still lacking, although regions of localized magnetosheath plasma have been found inside the magnetosphere on [*Lundin and Dubinin*, 1984; *Lundin et al.*, 2003]. The determination of the three-dimensional morphology of magnetosheath plasmoids made in this study can help to verify if the localized regions of magnetosheath plasma have properties consistent with penetration of such magnetosheath density enhancements.

[33] Plasmoids such as those reported in this paper may also have importance for solar wind-magnetosphere interaction, even when/if they do not penetrate into the magnetosphere. They may distort the magnetopause, similarly to the high-kinetic energy jets reported on by *Amata et al.* [2011], and for large plasmoids, the localized change in density and magnetic field may affect the local reconnection rate during southward IMF [*Borovsky*, 2008].

[34] The origins of the magnetosheath density enhancements are beyond the scope of this paper, but we note that there are three main possibilities; creation in the solar wind, at the bow shock or in the magnetosheath. A possible generation mechanism inside the magnetosheath would be the magnetic mirror instability, although magnetic mirror mode structures typically have smaller dimensions than those reported here [*Fazakerley and Southwood*, 1994; *Lucek et al.*, 2001; *Constantinescu et al.*, 2003]. The tendency of the plasmoids to orient themselves according to the direction of the direction of the bow shock/magnetopause quite far out in the magnetosheath is indication that the bow shock is the organizing factor. This points to generation here, or a modification of structures preexisting in the pristine solar wind. Some suggested mechanisms for producing localized density enhancements at the magnetosheath are hot-flow anomalies [*Omidi and Sibeck*, 2007; *Facskó et al.*, 2009], foreshock cavities [*Sibeck et al.*, 2002; *Turner et al.*, 2011], and interplanetary rotational discontinuities interacting with the bow shock [*Hubert and Harvey*, 2000]. A critical test for these mechanisms is to establish if plasmoids similar to those reported in the present paper exist already in the pristine solar wind. A search for such plasmoids in the solar wind is under way. If no such structures will be found in the solar wind, a more detailed investigation of the magnetosheath plasmoids,

such as their relation to magnetic field, temperature signatures, and other properties, is planned.

[35] **Acknowledgments.** T. Karlsson acknowledges funding from the Swedish Research Council, grant 2008–3717. We are grateful to P.-A. Lindqvist for discussions.

[36] Philippa Browning thanks Marius Echim and another reviewer for their assistance in evaluating this paper.

References

Amata, E., S. P. Savin, D. Ambrosino, Y. V. Bogdanova, M. F. Marcucci, S. Romanov, and A. Skalsky (2011), High kinetic energy density jets in the Earth's magnetosheath: A case study, *Planet. Space Sci.*, *59*, 482–494, doi:10.1016/j.pss.2010.07.021.

Balogh, A., et al. (2001), The Cluster magnetic field investigation: Overview of in-flight performance and initial results, *Ann. Geophys.*, *19*, 1207–1217, doi:10.5194/angeo-19-1207-2001.

Borovsky, J. E. (2008), The rudiments of a theory of solar wind/magnetosphere coupling derived from first principles, *J. Geophys. Res.*, *113*, A08228, doi:10.1029/2007JA012646.

Bostick, W. H. (1956), Experimental study of ionized matter projected across a magnetic field, *Phys. Rev.*, *104*, 292–299.

Bothmer, V., and R. Schwenn (1998), The structure and origin of magnetic clouds in the solar wind, *Ann. Geophys.*, *16*, 1–24, doi:10.1007/s00585-997-0001-x.

Brenning, N., T. Hurtig, and M. Raadu (2005), Conditions for plasmoid penetration across abrupt magnetic barriers, *Phys. Plasmas*, *12*, 1–10, doi:10.1063/1.1812277.

Burgess, D. (1995), Collisionless shocks, in *Introduction to Space Physics*, edited by M. G. Kivelson and C. T. Russel, pp. 129–163, Cambridge Univ. Press, Cambridge, U. K.

Constantinescu, O. D., K.-H. Glassmeier, R. Treumann, and K.-H. Fornacon (2003), Magnetic mirror structures observed by Cluster in the magnetosheath, *Geophys. Res. Lett.*, *30*(15), 1802, doi:10.1029/2003GL017313.

De Keyser, J., G. Gustafsson, M. Roth, F. Darrouzet, M. Dunlop, H. Rème, A. Fazakerley, P. Décréau, and N. Cornilleau-Wehrlin (2004), Reconstruction of the magnetopause and low-latitude boundary layer topology using Cluster multi-point measurements, *Ann. Geophys.*, *22*, 2381–2389.

Echer, E., W. D. Gonzales, and M. V. Alves (2006), Minimum variance of interplanetary coronal mass ejections around solar cycle 23 maximum, *Sol. Phys.*, *233*, 249–263, doi:10.1007/s11207-006-2380-7.

Echim, M. M., and J. F. Lemaire (2000), Laboratory and numerical simulations of the impulsive penetration mechanism, *Space Sci. Rev.*, *92*, 565–601, doi:10.1023/A:1005264212972.

Escoubet, C. P., A. Pedersen, R. Schmidt, and P.-A. Lindqvist (1997), Density in the magnetosphere inferred from ISEE-1 spacecraft potential, *J. Geophys. Res.*, *102*, 17,595–17,609, doi:10.1029/97JA00290.

Facskó, G., Z. Németh, G. Erdös, A. Kis, and I. Dandouras (2009), A global study of hot flow anomalies using Cluster multi-spacecraft measurements, *Ann. Geophys.*, *27*, 2057–2076, doi:10.5194/angeo-27-2057-2009.

Fazakerley, A. N., and D. J. Southwood (1994), Mirror instability in the magnetosheath, *Adv. Space Res.*, *14*, 65–68.

Gustafsson, G., et al. (1997), The electric field and wave experiment for the Cluster mission, *Space Sci. Rev.*, *79*, 137–156, doi:10.1023/A:1004975108657.

Hasegawa, H., M. Fujimoto, T.-D. Phan, H. Rème, A. Balogh, M. W. Dunlop, C. Hashimoto, and R. TanDokoro (2004), Transport of solar wind into Earth's magnetosphere through rolled-up Kelvin–Helmholtz vortices, *Nature*, *430*, 755–758, doi:10.1038/nature02799.

Hubert, D., and C. C. Harvey (2000), Interplanetary rotational discontinuities: From the solar wind to the magnetosphere through the magnetosheath, *Geophys. Res. Lett.*, *27*, 3149–3152, doi:10.1029/2000GL003776.

Hurtig, T., N. Brenning, and M. A. Raadu (2005), The role of high frequency oscillations in the penetration of plasma clouds across magnetic boundaries, *Phys. Plasmas*, *12*, 1–13, doi:10.1063/1.1812276.

Klein, L. W., and L. F. Burlaga (1982), Interplanetary magnetic clouds at 1 AU, *J. Geophys. Res.*, *87*, 613–624, doi:10.1029/JA087iA02p00613.

Lemaire, J. (1977), Impulsive penetration of filamentary plasma elements into the magnetospheres of the Earth and Jupiter, *Planet. Space Sci.*, *25*, 887–890, doi:10.1016/0032-0633(77)90042-3.

Lemaire, J., and M. Roth (1991), Non-steady-state solar wind-magnetosphere interaction, *Space Sci. Rev.*, *57*, 59–108, doi:10.1007/BF00195951.

Lepping, R. P., and K. W. Behannon (1980), Magnetic field directional discontinuities: 1. Minimum variance errors, *J. Geophys. Res.*, *85*, 4695–4703, doi:10.1029/JA085iA09p04695.

Lucek, E. A., M. W. Dunlop, T. S. Horbury, A. Balogh, P. Brown, P. Cargill, C. Carr, K.-H. Fornacon, E. Georgescu, and T. Oddy (2001), Cluster magnetic field observations in the magnetosheath: Four-point measurements of mirror structures, *Ann. Geophys.*, *19*, 1421–1428, doi:10.5194/angeo-19-1421-2001.

Lundin, R., and E. Dubinin (1984), Solar wind energy transfer regions inside the dayside magnetopause—I. Evidence for magnetosheath plasma penetration, *Planet. Space Sci.*, *32*, 745–755, doi:10.1016/0032-0633(84)90098-9.

Lundin, R., et al. (2003), Evidence for impulsive solar wind plasma penetration through the dayside magnetopause, *Ann. Geophys.*, *21*, 457–472, doi:10.5194/angeo-21-457-2003.

Ma, Z. V., J. G. Hawkins, and L. C. Lee (1991), A simulation study of impulsive penetration of solar wind irregularities into the magnetosphere at the dayside magnetopause, *J. Geophys. Res.*, *96*, 15,751–15,765, doi:10.1029/91JA01322.

Němeček, Z., J. Šafránková, L. Přech, D. G. Sibeck, S. Kokobun, and T. Mukai (1998), Transient flux enhancements in the magnetosheath, *Geophys. Res. Lett.*, *25*, 1273–1276, doi:10.1029/98GL50873.

Omidi, N., and D. Sibeck (2007), Formation of hot flow anomalies and solitary shocks, *J. Geophys. Res.*, *112*, A01203, doi:10.1029/2006JA011663.

Pedersen, A., P. Decreau, C.-P. Escoubet, G. Gustafsson, H. Laakso, P.-A. Lindqvist, B. Lybekk, A. Masson, F. Mozer, and A. Vaivads (2001), Four-point high time resolution information on electron densities by the electric field experiments (EFW) on Cluster, *Ann. Geophys.*, *19*, 1483–1489, doi:10.5194/angeo-19-1483-2001.

Pedersen, A., et al. (2008), Electron density estimations derived from spacecraft potential measurements on Cluster in tenuous plasma regions, *J. Geophys. Res.*, *113*, A07S33, doi:10.1029/2007JA012636.

Phan, T.-D., G. Paschmann, W. Baumjohann, N. Sckopke, and H. Lühr (1994), The magnetosheath region adjacent to the dayside magnetopause: AMPTE/IRM observations, *J. Geophys. Res.*, *99*, 121–141, doi:10.1029/93JA02444.

Rème, H., et al. (2001), First multispacecraft ion measurements in and near the Earth's magnetosphere with the identical Cluster Ion Spectrometry (CIS) experiment, *Ann. Geophys.*, *19*, 1303–1354, doi:10.5194/angeo-19-1303-2001.

Savin, E., et al. (2008), High energy jets in the Earth's magnetosheath: Implications for plasma dynamics and anomalous transport, *JETP Lett.*, *87*(11), 593–599.

Seon, J., S. M. Park, K. W. Min, L. A. Frank, W. R. Paterson, and K. W. Ogilvie (1999), Observations of density fluctuations in Earth's magnetosheath with Geotail and Wind spacecraft, *Geophys. Res. Lett.*, *26*, 959–962, doi:10.1029/1999GL900131.

Shevyrev, N. N., G. N. Zastenker, P. E. Eiges, and J. D. Richardson (2006), Low frequency waves observed by Interball-1 in foreshock and magnetosheath, *Adv. Space Res.*, *37*, 1516–1521, doi:10.1016/j.asr.2005.07.072.

Sibeck, D. G., and J. T. Gosling (1996), Magnetosheath density fluctuations and magnetopause motion, *J. Geophys. Res.*, *101*, 31–40, doi:10.1029/95JA03141.

Sibeck, D. G., R. E. Lopez, and E. C. Roelof (1991), Solar wind control of the magnetopause shape, location, and motion, *J. Geophys. Res.*, *96*, 5489–5495, doi:10.1029/90JA02464.

Sibeck, D. G., et al. (1999), Plasma transfer processes at the magnetopause, *Space Sci. Rev.*, *88*, 207–283, doi:10.1023/A:1005255801425.

Sibeck, D., T.-D. Phan, R. Lin, R. P. Lepping, and A. Szabo (2002), Wind observations of foreshock cavities: A case study, *J. Geophys. Res.*, *107*(A10), 1271, doi:10.1029/2001JA007539.

Sonnerup, B. U. Ö., and L. J. Cahill (1967), Magnetopause structure and attitude from Explorer 12 observations, *J. Geophys. Res.*, *72*, 171–183, doi:10.1029/JZ072i001p00171.

Sonnerup, B. U. Ö., and M. Scheible (1998), Minimum and maximum variance analysis, in *Analysis Methods for Multi-Spacecraft Data*, *ISSI Sci. Rep. Ser.*, vol. 1, edited by G. Paschmann and P. Daly, pp. 185–220, Eur. Space Agency/Int. Space Sci. Inst., Nordwijk, Netherlands.

Stasiewicz, K. (1993), Finite Larmor radius effects in the magnetosphere, *Space Sci. Rev.*, *65*, 221–252, doi:10.1007/BF00754509.

Trotignon, J. G., J. L. Rauch, P. M. E. Décréau, P. Canu, and J. Lemaire (2003), Active and passive plasma wave investigations in the Earth's environment: The Cluster/Whisper experiment, *Adv. Space Res.*, *31*, 1449–1454, doi:10.1016/S0273-1177(02)00959-6.

Turner, D. L., S. Eriksson, T. D. Phan, V. Angelopoulos, W. Tu, W. Liu, X. Li, W.-L. Teh, J. P. McFadden, and K.-H. Glassmeier (2011), Multispacecraft observations of a foreshock-induced magnetopause disturbance exhibiting distinct plasma flows and an intense density compression, *J. Geophys. Res.*, *116*, A04230, doi:10.1029/2010JA015668.

Wessel, F. J., R. Hong, J. Song, A. Fisher, N. Rostoker, A. Ron, and R. Y. Fan (1988), Plasmoid propagation in a transverse magnetic field and in a magnetized plasma, *Phys. Fluids*, *31*, 3778–3784, doi:10.1063/1.866897.

Zastenker, G. N., M. N. Nozdrachev, Z. Nemecek, J. Safrankova, K. I. Paularena, J. D. Richardson, R. P. Lepping, and T. Mukai (2002), Multispacecraft measurements of plasma and magnetic field variations in

the magnetosheath: Comparison with Spreiter models and motion of the structures, *Planet. Space Sci.*, *50*, 601–612, doi:10.1016/S0032-0633(02)00039-9.

N. Brenning and T. Karlsson, Space and Plasma Physics, School of Electrical Engineering, Royal Institute of Technology, S-10044 Stockholm, Sweden. (tomas.karlsson@ee.kth.se)

G. Facsko, Earth Observation Unit, Finnish Meteorological Institute, FI-00101 Helsinki, Finland.

H. Nilsson, Swedish Institute of Space Physics, S-981 28 Kiruna, Sweden.

J.-G. Trotignon and X. Vallières, Laboratoire de Physique et Chimie de l'Environnement et de l'Espace, CNRS, F-45071 Orléans, France.